

High-Throughput Characterization of Pattern Formation in Symmetric Diblock Copolymer Films

ARCHIE P. SMITH, JACK F. DOUGLAS, J. CARSON MEREDITH,* ERIC J. AMIS, ALAMGIR KARIM

Polymers Division, National Institute of Standards and Technology, Mail Stop 8542, Gaithersburg, Maryland 20899

Received 17 November 2000; revised 10 May 2001; accepted 21 May 2001

ABSTRACT: Surface-pattern formation in thin block copolymer films was investigated by utilizing a high-throughput methodology to validate the combinatorial measurement approach and to demonstrate the value of the combinatorial method for scientific investigation. We constructed measurement libraries from images of subregions of block copolymer films having gradients in film thickness and a range of molecular mass, M . A single gradient film covers a wide range of film morphologies and contains information equivalent to a large number of measurements of films having a fixed thickness, h . Notably, the scale of the surface patterns is generally much larger than the molecular dimensions so that the interpretation of the patterns is more subtle than ordering in bulk block copolymer materials, and there is no predictive theory of this type of surface-pattern formation. We observed a succession of surface patterns that repeat across the film with increasing h [extended smooth regions, regions containing circular islands, labyrinthine (“spinodal”) patterns, holes, and smooth regions again]. The extended smooth regions and the labyrinthine patterns appear to be novel features revealed by our combinatorial study, and these patterns occurred as bands of h that were quantized by integral multiples of the bulk lamellar period, L_o . The magnitude of the height gradient influenced the width of the bands, and the smooth regions occupied an increasing fraction of the film-surface area with an increasing film gradient. The average size of the spinodal patterns, λ , was found to scale as $\lambda \sim L_o^{-2.5}$ or $\lambda \sim M^{-1.65}$ and reached a limiting size at long annealing times. The hole and island features had a size comparable to λ , and their size likewise decreased with increasing M . The smooth regions were attributed to an increase in the surface-chain density in the outer brush-like block copolymer layer with increasing h , and the scaling of λ with M was interpreted in terms of the increasing surface elasticity with M . © 2001 John Wiley & Sons, Inc. *J Polym Sci Part B: Polym Phys* 39: 2141–2158, 2001

Keywords: combinatorial measurements; block copolymer; thin film; surface pattern

INTRODUCTION

Combinatorial analysis, in conjunction with high-throughput multivariate measurements, is a new and rapidly developing approach to materials sci-

ence research. This methodology is made possible by the development of the computational resources needed to store and analyze the large amounts of information that such studies naturally generate. This method involves the creation of large “material libraries” and high-throughput screening techniques that allow the efficient exploration of the multiparameter space governing complex physical phenomena. This approach can be utilized to rapidly identify regions of parameter space where particularly interesting phenom-

* Present address: School of Chemical Engineering, Georgia Institute of Technology, Atlanta, GA 30332

Correspondence to: A. Karim (E-mail: alamgir.karim@nist.gov)

Journal of Polymer Science: Part B: Polymer Physics, Vol. 39, 2141–2158 (2001)
© 2001 John Wiley & Sons, Inc.

ena occur, and the method is also helpful in establishing basic parameter trends that assist in gaining an understanding of the origin of the observed phenomena. This information is not only useful in the practical design of new materials^{1,2} but can contribute greatly in the development and testing of theoretical models.

Combinatorial methodologies have revolutionized the pharmaceutical industry because of their capacity to bring new drugs to the market in a timely, cost-effective manner.^{3,4} The application of combinatorial principles to materials science characterization likewise promises to influence the future direction of research and development. Application of the combinatorial process is already occurring in the discovery of new catalysts and in a wide variety of inorganic materials investigations utilizing semiconducting, phosphoric, and superconducting materials.⁵

The characterization of the physical properties of polymeric materials is one area where combinatorial methods are just beginning to find application.^{6–9} Many of the techniques used to prepare libraries for inorganic materials are inapplicable to organic and polymeric materials; thus, new strategies must be developed that are suitable to these materials. As an initial application of combinatorial methods to organic materials, a technique has been developed to create polymer thin films with continuous gradients in film thickness and composition.^{7–9} In the present article, the utility of this technique is demonstrated by investigating the well-studied phenomenon of surface-pattern formation in block copolymer films. In addition to reproducing former results, our investigation has uncovered important new aspects of block copolymer film-pattern formation that should be helpful in the development of a theory of this type of surface-pattern formation.

Symmetric diblock copolymers are composed of polymer components of nearly equal molecular mass joined at a covalent chemical junction. Previous studies^{10–33} have shown that in ordered thin films of these materials, the polymer-surface interactions induce the formation of lamellae parallel to the substrate surface that have a thickness nearly equal to the bulk equilibrium lamellae spacing, L_o . When one block segregates to both the substrate and air interfaces, smooth films are formed with a total thickness $h_s = mL_o$, where m is an integer. Conversely, smooth films of thickness $h_s = (m + \frac{1}{2})L_o$ are observed when one block segregates to the substrate and the other to the air interface. In the case where film

thickness h deviates from h_s , the excess material forms an incomplete surface lamella in the form of islands or holes with height L_o with the nature and percentage of surface coverage of these features dependent on the deviation of h from h_s . This dependence of the surface morphology on h is exploited to demonstrate the efficacy of combinatorial methods applied to polymer characterization by creating thickness gradient thin films of symmetric polystyrene-*b*-poly(methyl methacrylate) (PS-*b*-PMMA) copolymers of different molecular masses M . Of primary interest in the present study is the location and nature of transitions in the surface-pattern morphology, the effect of the gradient slope on the morphology, and factors that govern the lateral size of the surface patterns.

LIBRARY CREATION AND CHARACTERIZATION

To create thin-film thickness gradient libraries, a specially designed automated solution flow coater has been developed. This flow coater, shown in Figure 1(a), is based on a computer-controlled linear motion stage, which moves at variable speeds to create the film-thickness gradient. The substrates utilized for these gradients are Si wafers (10 cm diameter, Polishing Corp. of America³⁴) that have been cleaned with the standard "Piranha-etch" technique to form a SiO_x/SiOH surface layer.³⁵ After cleaning, the Si wafer was secured to the robotic stage, and a 30-mm-wide knife edge was placed $\approx 300 \mu\text{m}$ above the substrate surface at an approximate 5° angle with respect to the substrate. Approximately 50 μL of polymer solution (mass fraction 1–10%) were subsequently placed under the knife edge, and the robotic stage was driven with constant acceleration spreading the solution. Solvent evaporation occurs in a matter of seconds, producing a thin film with thickness related to the stage velocity (i.e., higher velocity produces thicker films). Typical thin films are 25–35 mm in length and have thickness gradients of 40–50 nm, although these values can be varied. Control of the initial film thickness and gradient slope is achieved by modifying the solution concentration, solution volume, solvent, knife-edge height, and stage acceleration. Films as thin as 2 nm and as thick as 10 μm with gradient ranges as small as 10 nm and as large as 5 μm have been produced with this methodology.

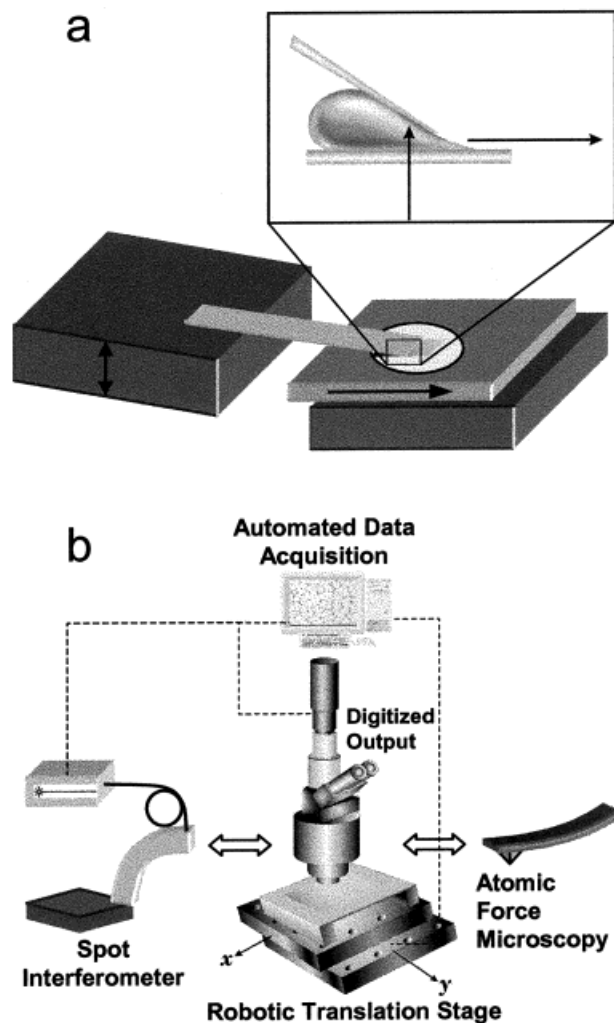


Figure 1. Diagrams of the basic elements of high-throughput polymer film measurements: (a) automated flow coater used to make films having a gradient in thickness and (b) UV-vis interferometry, optical microscopy, and AFM used to characterize the h -gradient films.

The film thickness of the gradient library samples was measured by a Filmetrics F20 ultraviolet-visible (UV-vis) interferometer with a 0.5-mm spot diameter and a standard uncertainty of ± 1 nm for a 500 nm film [shown in Fig. 1(b)]. This interferometer is connected to an automated translation stage where measurements are acquired at intervals across the sample (usually having 2–3 mm spacing). These thickness measurements are used to create a two-dimensional library of the film thickness, which can be used to create a thickness contour map of the sample. Figure 2(a) shows a thickness map for a film prepared from a solution with a mass fraction

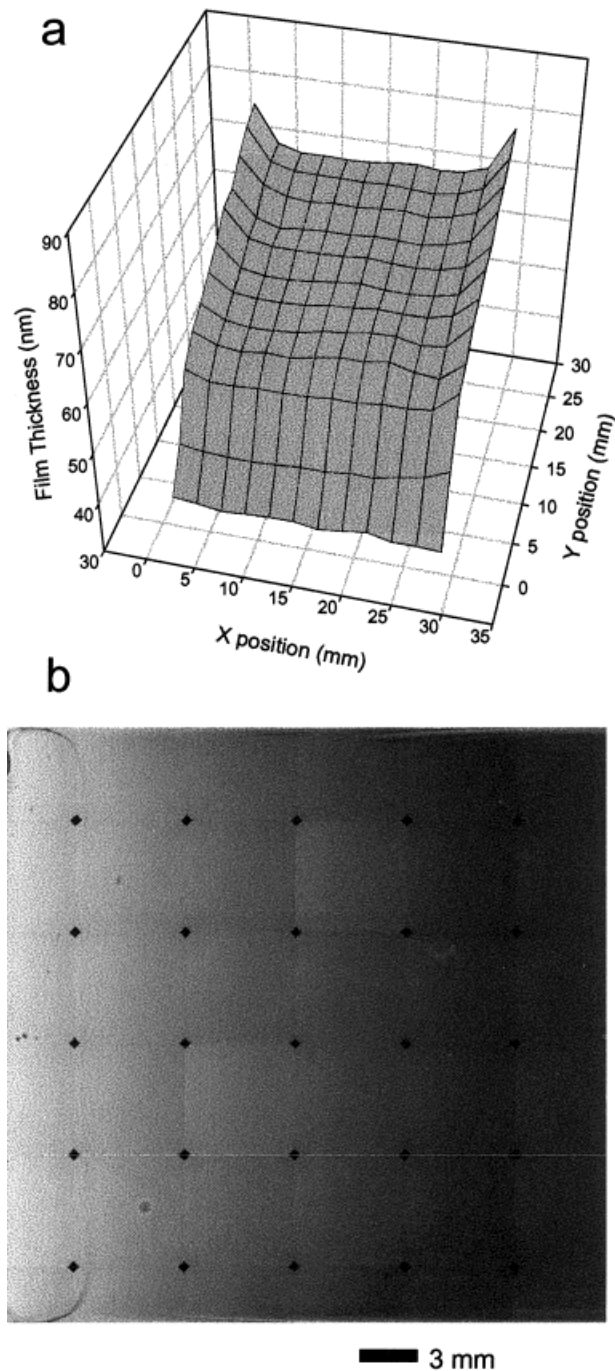


Figure 2. (a) Plot of the film thickness for a gradient library. The thickness measurements were performed by spot interferometry and acquired on a 2.5-mm grid. (b) Composite optical micrograph of a gradient film library showing typical film features. Thicker regions are represented by darker colors. Dark diamonds are artifacts of the CCD digitization.

Table I. Molecular Characteristics and Lamella Thickness (L_o) for the Block Copolymers in This Study (Errors Given Are the Standard Uncertainty)

Label	M_n S Block ³⁷ (g/mol)	M_n MMA Block (g/mol)	M_w/M_n	L_o Calculated ¹⁴ (nm)	L_o Measured (nm)
26k	12,800	12,900	1.05	17.1	17.8 ± 0.8
51k	25,300	25,900	1.06	26.8	30.2 ± 0.8
104k	50,000	54,000	1.04	42.4	42.3 ± 1.4

of 4% polymer and a stage acceleration of 0.175 mm/s². In this example, thickness measurements were acquired with 2.5-mm spacing across a library approximately 30 mm in length with a thickness varying between 35 and 75 nm. Flow behavior near the free boundary of the knife edge produces a slight thickening of the film (\approx 5 nm) within \approx 2 mm of each edge, and this region is excluded from consideration. The inner region, however, has a nearly uniform thickness gradient that can be utilized for quantitative experimental investigations. For example, the relative thickness variation in the center of the gradient (orthogonal to the thickness gradient direction) shown in Figure 2(a) is less than 4% at any position along the gradient. The viscoelastic nature of the polymer film ensures that the gradients remain stable for small spatial scales and long time-scales.³⁶

Optical microscopy [OM, depicted in Fig. 1(b)] was also utilized to characterize the gradient libraries. A Kodak Megaplug camera (1024 × 1024, 8-bit pixels) was connected to a Nikon Optiphot 2 microscope operating in the reflection mode. The microscope's standard sample stage was replaced with a motorized two-dimensional translation stage possessing a 5-cm range of motion and a 0.5- μ m resolution. A computer synchronously controls the translation stages and acquires digital images from the CCD while scanning across the sample. These micrographs can be assembled together to form a composite image of the entire library, and an example of this is found in Figure 2(b). In this figure, low-magnification optical micrographs (25 \times) are acquired from a film cast with a mass fraction of 2% polymer and assembled to show the film structure of the entire library. The contrast is provided by the optical interference within the thin film, and the darker shades represent thicker areas for films of this thickness range. The gradient library creation methodology described in this work allows for combinatorial samples possessing up to 100 dis-

tinct state points ($\Delta h = 0.5$ nm) per library. This large amount of data greatly expands the potential for scientific investigation and practical characterization of polymer-film properties.

SYMMETRIC DIBLOCK COPOLYMER MORPHOLOGY

To demonstrate the advantages of using the combinatorial libraries previously described for studying block copolymers, thin-film gradient libraries of the symmetric diblock copolymer poly(styrene-*b*-methyl methacrylate) (PS-*b*-PMMA, Polymer Source Inc.) were created. The molecular characteristics³⁷ of the PS-*b*-PMMA copolymers (as provided by the supplier) are given in Table I. Unreacted homopolymer contamination is estimated to be less than 4% based on gel permeation chromatographic and NMR data provided by the supplier. Solutions with mass fractions of 2–5% in toluene were used to create gradient film libraries on Si wafers with SiO_x/SiOH surface layers. Up to four libraries having different initial h , gradient slopes, and molecular masses were placed on a single 100 mm Si wafer to extend the h range and eliminate experimental processing variability. Interferometric measurements, as previously described, were performed on the as-cast films, and the libraries subsequently annealed at 170 °C for up to 96 h under vacuum. After annealing, the morphology of the resultant films was characterized by OM and atomic force microscopy (AFM) on a Digital Nanoscope Dimension 3100.

Previous work^{12–14,18} has determined that when thin films of PS-*b*-PMMA are placed on Si with a SiO_x/SiOH surface layer and annealed, the PMMA block preferentially segregates to the substrate, whereas the PS block segregates to the air interface. This behavior results in smooth films with $h_s = (m + \frac{1}{2})L_o$ for this copolymer and incomplete surface lamellae with various surface patterns when the film deviates from this thick-

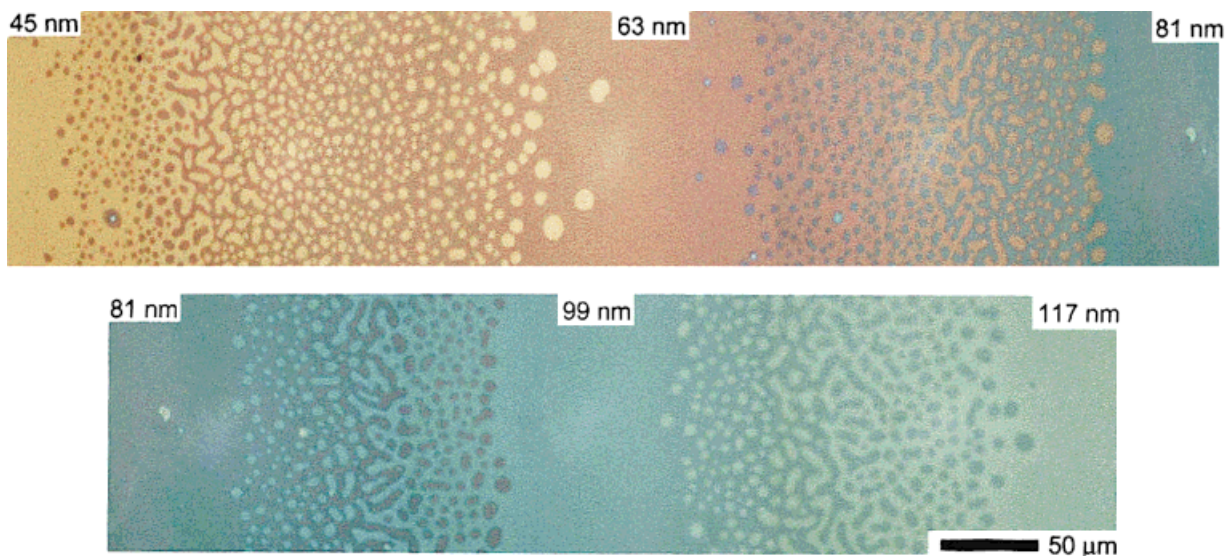


Figure 3. True color optical micrograph of a continuous 26k PS-*b*-PMMA gradient film. Film was annealed for 6 h at 170 °C, and the image shows the addition of four successive lamellae to the block copolymer film with increasing thickness. Labels indicate the approximate position of $h_s = (m + \frac{1}{2})L_o$, where $m = 2-6$. The lower section is a continuation of the upper section.

ness. These observations were acquired from studying a number of individual samples, each having a discrete h such that the sample set spanned the h range of interest. By utilizing the thickness gradient libraries used here, the complete, continuous addition of successive lamellae on a single sample can be observed directly, as shown in Figure 3. True-color OM micrographs obtained from a continuous 26k PS-*b*-PMMA gradient film annealed for 6 h at 170 °C are assembled together to form a montage showing the addition of four lamellae. This micrograph is obtained near the gradient film edge to compress the lateral scale, and h varies nonlinearly from $\approx (45$ to $117)$ nm over a distance of ≈ 1.1 mm. Labels denote h at the approximate locations of h_s for $m = 2, 3, 4, 5,$ and 6 . The island and hole morphologies observed in this micrograph are consistent with previous observations from samples having a fixed h .^{10,15,16,25,26} Identification of the labyrinthine morphology separating the island and hole patterns and observation of the width of the bands where the films remain smooth are apparently new results that have not been reported previously.

A more detailed picture of the morphology evolution with increasing h is presented in Figure 4. This figure shows OM micrographs obtained from a continuous 51k PS-*b*-PMMA gradient library

annealed for 30 h at 170 °C, placed together to form a composite image of the film-surface morphology. These micrographs were obtained from a section of a gradient ≈ 2.5 mm in length having an initial h range of $\approx 70-100$ nm (or equivalently $2.5-3.5L_o$ for this molecular mass). Contrast is provided by the thin-film optical interference, and the darker gray corresponds to the $3.5L_o$ layer thickness. As h increases above 70 nm, discrete islands initially form [shown in the enlargement in Fig. 4(a)] and adopt a circular appearance as a result of surface-energy minimization, as previously observed.^{16,17} Increasing h further causes the islands to grow in size and consolidate until a labyrinthine pattern of islands and holes forms [Fig. 4(b)] near certain critical film thicknesses, h_c . This morphology resembles spinodal decomposition in polymer blends³⁸ and spinodal dewetting³⁹ patterns in other polymeric systems so that we term these “spinodal patterns.” A “phase-separation” model of block copolymer pattern formation has been proposed⁴⁰⁻⁴² with the variation of film height relative to a critical value playing the role of an order parameter, and this model is considered subsequently. With a further increase in h , the morphology undergoes a “phase inversion” where the islands become continuous and form the next lamella ($h = 3.5L_o$) with large irregular shaped holes down to the previous

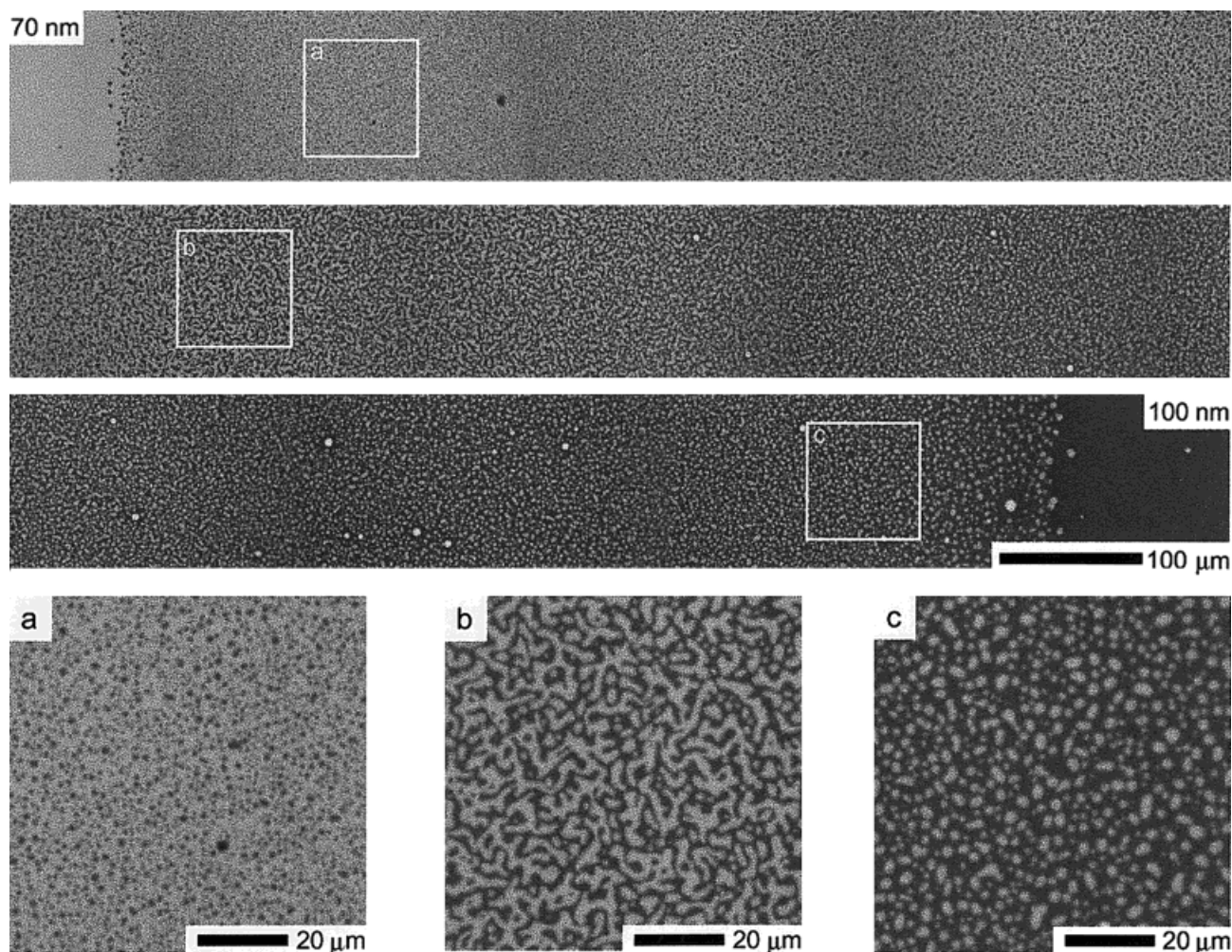


Figure 4. Composite optical micrograph of a continuous 51k PS-*b*-PMMA film annealed for 30 h at 170 °C. The unannealed film thickness range is roughly 70–100 nm (or 2.5–3.5 L_o) with the new lamella appearing dark relative to the underlying layer. The enlargements show (a) islands of the new lamella on the surface of the existing lamella, (b) a labyrinthine island/hole pattern (“spinodal pattern”), and (c) holes in the new lamella down to the underlying lamella. The bright white areas correspond to film dewetting.

lamella “surface” ($h = 2.5L_o$). The size and number of holes decrease as h increases further [Fig. 4(c)] until the holes eventually disappear, leaving a smooth film when $h = 3.5L_o$ (≈ 100 nm for this M). The morphologies observed in this figure are next investigated at higher resolution using AFM.

Figure 5 depicts AFM micrographs obtained from 51k PS-*b*-PMMA gradient films annealed for 6 h at 170 °C, where the brighter colors correspond to higher topography. The micrographs were acquired from two gradient libraries with h between 35 and 70 nm and 65 and 110 nm, respectively. This figure illustrates the morphological variation with h observed in Figure 4 but at a

higher magnification. The h values given in the figure correspond to $h \approx 1.5$ – $3.5L_o$ and are determined from interferometer measurements on the unannealed sample with an estimated error of ± 2 nm. These micrographs show a smooth surface morphology ($h = 42$ nm), followed by the formation of circular islands ($h = 46$ nm, 51 nm) that become larger and irregular in shape ($h = 54$ nm). The islands eventually grow large enough to join together to form the next continuous lamella with large, irregular holes down to the previous lamella ($h = 61$ nm, 63 nm). These holes become smaller and more circular ($h = 68$ nm) followed by an increase in size accompanied by

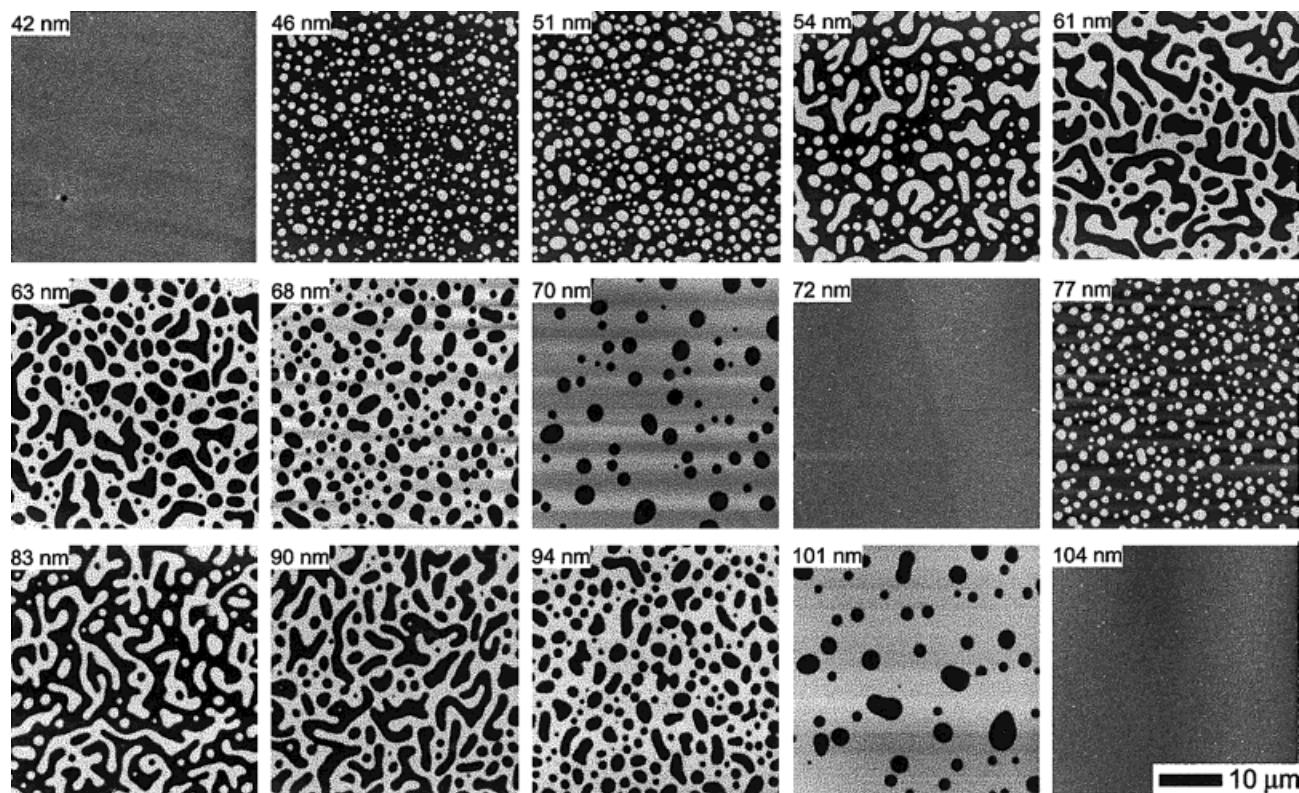


Figure 5. AFM micrographs showing the morphology variation with h . Bright areas correspond to the higher topography of the 51k PS-*b*-PMMA samples annealed for 6 h at 170 °C. Labels indicate the unannealed film thickness with an estimated standard uncertainty of ± 2 nm. These micrographs show that successive lamellae form according to the same pattern-formation series (islands, spinodal patterns, holes, etc.).

a decrease in number (70 nm) as h is further increased. The holes eventually disappear to reform a smooth surface ($h = 72$ nm). This sequence of surface-pattern evolution is then repeated as h increases from 72 to 104 nm. In addition to illustrating the detailed nature of the transition from island to spinodal to hole-pattern formation, these micrographs show that the morphological pattern repeats for each additional lamella added to the film. Although this sequence of pattern formation is only shown for two lamellae, it is repeatedly observed in films with h up to $6.5L_o$. AFM is also used to measure L_o from multiple points across the films, and these values are given in Table I along with the calculated standard deviation. The measured L_o values agree well with those calculated from the previously determined¹⁴ empirical relation $L_o \propto M^{0.66}$ (Table I), corresponding to the expected strong segregation scaling.⁴³ This agreement, as well as the similarity in morphology between the combinatorial samples and the uniform h samples observed

previously, provide an important consistency check for the continuous gradient methods utilized for the present experiment.

We next focus attention on aspects of the surface morphology observed in the gradient samples that have not been previously identified in uniform h samples. The first feature of interest is the labyrinthine island/hole morphology (“spinodal pattern”), shown in Figures 4(b) and 5 (83 nm micrograph), and the critical film thickness, h_c , where this morphology occurs. This morphology type is observed for all annealing times and should not be confused with transient patterns observed at short times in a thickness regime that later evolves into islands or holes.¹⁷ Similar labyrinthine patterns have also been observed in block copolymer films on patterned substrates.^{32,33} As seen in Figure 4, the area where the spinodal pattern exists is quite narrow relative to the entire lamellar width, corresponding to a small film-thickness regime relative to L_o . Utilizing OM and AFM, the location of the spinodal

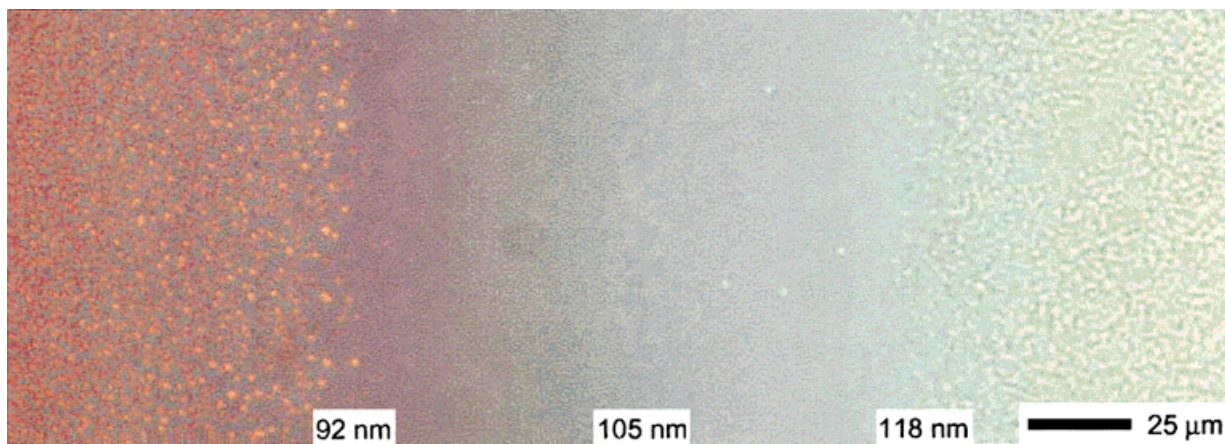


Figure 6. True color optical micrograph across smooth band. The image is of a 104k PS-*b*-PMMA gradient film. The outer block copolymer lamella becomes increasingly stretched as the chain density increases with increasing h and the layer expands as a result of increased interchain interactions.

pattern was determined to be at $0.41 \pm 0.03L_o$ above the smooth film thickness h_s , or equivalently $h_c = [m + (0.91 \pm 0.03)]L_o$. The value of h_c is invariant with respect to M within experimental uncertainty and stable under the annealing conditions applied in the present work. Of significance is the fact that the h_c value is not exactly $0.5L_o$ above h_s , such that the hole morphologies occupy a larger fraction of the lamellar morphology relative to the island morphologies. This finding indicates that the holes are a more energetically favorable surface morphology than the islands, as previously suggested.^{17,26}

The next feature of interest is the smooth regions between the island and hole-surface patterns shown in Figures 3 and 4. These regions are centered about h_s (within experimental error) and are defined by abrupt transitions separating the areas where islands and holes exist. The smooth regions account for a large percentage of the gradient film area and thus correspond to a range of h deviating significantly from h_s , and this fraction becomes increasingly large as the h gradient is increased. These smooth regions are hypothesized to arise from deformations in the outer block copolymer layer and were investigated experimentally. The hypothesis of chain expansion and compression of the surface block copolymer layer relative to L_o implies an h variation across the smooth region that should be detectable. The continuous gradient method utilized here allows the measurement of this h variation in the smooth “transition” region illustrated in Figure 6. This figure shows a true-color OM

micrograph of a 104k PS-*b*-PMMA gradient film with the film thickness indicated. The sample was annealed for 22 h at 170 °C, and the micrograph was obtained near the edge of the sample to compress the lateral dimension of the smooth region. The orange features on the left of Figure 6 are holes, whereas the green/yellow features on the right are islands. The island and holes lack definition in this micrograph because their size is near the resolution limit of optical microscopy. The color of the smooth region between the holes and islands varies from purple to blue/green because of interference changes caused by increasing h . This color change indicates an h variation across the smooth region of ≈ 25 nm centered about 105 nm (h_s for $m = 2$) for this sample.

To further quantify the film-thickness change across these smooth regions, gradients were annealed for 30 h at 170 °C to obtain approximate “steady-state” (or at least very slowly varying) film patterns. Positions of the interface between the holes and smooth areas as well as between the smooth region and islands were recorded. The unannealed h of these positions was then utilized to determine the change in film thickness (Δh) across the entire smooth region. Because h_s is found to be near the smooth region center, $\Delta h/2$ is the height deviation at the edges of the smooth film region relative to the smooth region center, h_s . The values of $\Delta h/2$ obtained for each M investigated are listed in Table II, along with the change in this quantity relative to L_o , $\delta h = (\Delta h/2)/L_o$. The data in Table II show that δh is nearly *invariant* within standard uncertainty for the

Table II. Measured Parameters for the Smooth Regions in the Block Copolymer Morphology as a Function of M (Errors Given Are the Standard Uncertainty)

M_n (kg/mol)	$\Delta h/2$ (nm)	$\delta h = (\Delta h/2)/L_o$	ε_c (nm/mm)
26k	2.1 ± 0.7	0.12 ± 0.03	720 ± 50
51k	4.2 ± 0.5	0.14 ± 0.01	2400 ± 300
104k	5.8 ± 0.8	0.14 ± 0.01	3300 ± 400

films studied, regardless of the block copolymer M . Furthermore, no statistically significant variation in δh was found for $h < h_s$ and $h > h_s$ or with an increase in the total number of lamellae, up to films having a thickness $h \approx 6.5L_o$. This h independence of δh directly supports our hypothesis that the chain deformation is confined to the outer block copolymer layer because δh would otherwise depend on the total number of lamellae.

We next examined the effect of the gradient slope, $\varepsilon \equiv \Delta h/\Delta w$, where w is the width of the region under consideration, on the morphology of the system. Although the gradients achievable with the gradient flow coater are limited, we can investigate higher gradients by using a combination of the cast gradients in the central regions of the film and the steeper, nonlinear gradient structures located at the film edges. The influence of ε on the block copolymer surface morphology is demonstrated by comparing Figures 3, 4, and 7. Figure 4 demonstrates that the island and hole morphologies are significantly wider than the smooth surface areas for $\varepsilon \approx 10$ nm/mm. This morphology trend is also observed for slopes as low as ≈ 1 nm/mm (not shown here) with a corresponding decrease in the fraction of the smooth regions relative to the regions where the hole and island morphologies are observed. Figure 3 shows the morphology in a film where $\varepsilon \approx 80$ nm/mm and demonstrates the increase in the width of the smooth region relative to the island and hole patterns with increasing ε . Micrographs of films with even higher ε are shown in Figure 7, illustrating the morphological effect of changing ε in the high-gradient regime. These micrographs were obtained from 26k PS-*b*-PMMA films annealed for 30 h at 170 °C. Figures 7(a,b) are optical micrographs of films with ε of approximately (a) 150 nm/mm (uniform across the sample) and (b) 500 nm/mm (left side) to 750 nm/mm (right side). Figure 7(c) is an AFM micrograph of a film

with the steepest gradient, $\varepsilon \approx 1800$ nm/mm with a line scan of the micrograph indicating the film h change. Notably, the step-like height variation is only apparent in films having steep gradients. For completeness, we note that $\varepsilon \approx 1$ nm/mm in Figure 5 and $\varepsilon \approx 180$ nm/mm in Figure 6. We next consider the crossover between the low- and high-gradient film morphologies.

The micrographs shown in Figures 3, 4, and 7 demonstrate that the smooth regions centered about h_s become an increasingly large part of the total lamella morphology as ε increases, until the lamellae eventually adopt a step-like morphology. To further investigate this behavior, the width of the smooth region, w_s , and the width of the entire lamella, w_L , as shown in Figure 7, were measured as a function of ε from samples annealed for 30 h at 170 °C. Figure 8 depicts a plot of the ratio w_s/w_L as a function of ε for all three molecular masses investigated. Inspection of this plot reveals that this ratio goes to its maximum value of unity (corresponding to adoption of the step-like morphology) with increasing ε , independent of M . Once a ratio of unity is attained, a further increase of ε does not alter the step morphology, but

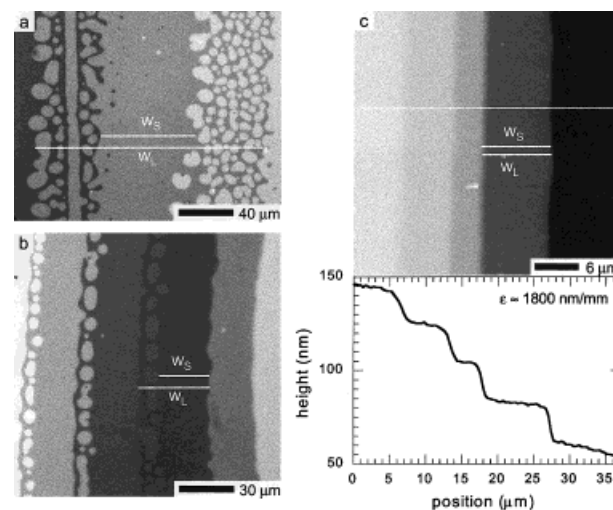


Figure 7. Influence of ε on surface-pattern formation of 26k PS-*b*-PMMA samples: (a) optical micrograph of an area with $\varepsilon \approx 150$ nm/mm showing that the smooth area width (w_s) is a larger fraction of the entire lamella morphology width (w_L) than in Figures 3 and 4, (b) optical micrograph of regions with $\varepsilon \approx 500$ nm/mm (left side) and $\varepsilon \approx 750$ nm/mm (right side) showing how the morphology becomes steplike with increasing slope, and (c) AFM micrograph of a defect with $\varepsilon \approx 1800$ nm/mm with a line scan (denoted as the white line) demonstrating the steplike nature of the lamellae above the critical slope values.

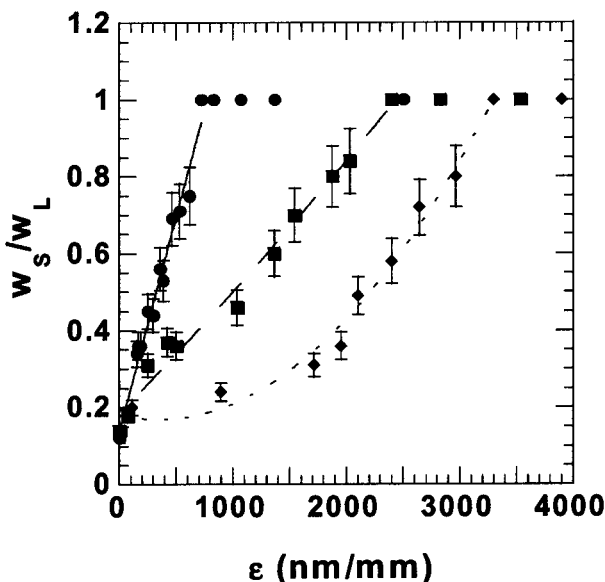


Figure 8. Plot of the ratio w_S/w_L versus ϵ for the 26k (●, solid line), 51k (■, dashed line), and 104k (◆, dotted line) M samples showing how the relative width of the smooth area increases with increasing gradient slope. The slope at which w_S/w_L first equals 1 increases with increasing M . Lines serve as a guide to the eye, and error bars are the standard uncertainty.

the width of the step decreases. The value of ϵ where the ratio w_S/w_L initially plateaus to unity, ϵ_c , increases with increasing M . The measured ϵ_c values (see Table II) correspond to the point where islands or holes can no longer form as a result of the steep gradient, and the step-like film morphology is then adopted. This behavior is discussed in more detail subsequently.

The next aspect of the block copolymer films investigated is the effect of the copolymer molecular mass on the surface-pattern formation and evolution. Changes in M have previously been found¹³ to affect the equilibrium lamellar thickness L_o (as described previously) and the kinetics of lamellar formation and evolution. In addition, we observed an M dependence on the lateral (in-plane) size scale of the spinodal surface patterns, as demonstrated in Figure 9. AFM micrographs obtained from PS-*b*-PMMA gradient films with M 's of 26k [Figs. 9(a,d)], 51k [Figs. 9(b,e)], and 104k [Figs. 9(c,f)] annealed at 170 °C for 6 h [Figs. 9(a–c)] and 30 h [Figs. 9(d–f)] are shown. These images were obtained at constant magnification near $h \approx h_c$ where the spinodal patterns occur, and a line scan obtained from the area designated by the white line is plotted below each micrograph. The effects of M on the inplane surface-

pattern dimensions are visible for the samples annealed for only 6 h [shown in Figs. 9(a–c)]. The lateral pattern scale in the 26k, 51k, and 104k films become increasingly small with increasing M . Further annealing of these materials for 30 h produces an increase in the size of the lateral pattern scale, but the significantly smaller morphology found for the high M samples is retained.

To quantify the M dependence of the surface-pattern sizes and evolution demonstrated in Figure 9, two-dimensional fast-Fourier transforms of micrographs obtained from samples annealed up to 96 h were performed. The circular average of the transform data yielded a peak in the intensity data at wavevector \mathbf{q}^* . A characteristic size, λ , defined as $\lambda \equiv (\mathbf{q}^*)^{-1}$, was also calculated. Figure 10 shows a plot of this calculated λ as a function of annealing time for films of all three molecular masses annealed up to 96 h. The plot shows that the differences in λ because of M observed in Figure 9 are retained for long annealing times. Therefore, the lateral scale of the surface patterns always decreases strongly with increasing M for the times investigated. In addition, Figure 10 illustrates that the lateral size of the morphology ceases to evolve and becomes nearly stationary

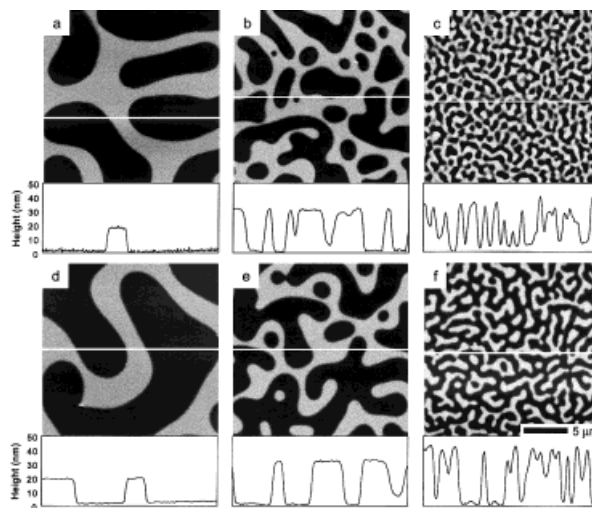


Figure 9. Molecular mass dependence of the block copolymer spinodal pattern size. AFM images: (a,d) 26k, (b,e) 51k, and (c,f) 104k of symmetric PS-*b*-PMMA copolymer films annealed for (a–c) 6 h and (d–f) 30 h at 170 °C. The 26k (a,d) sample has the largest surface features, whereas the higher M samples have smaller surface features. Line scans from each micrograph (denoted by white lines) demonstrate how the pattern shoulders become more rounded, reducing the roughness of the sample.

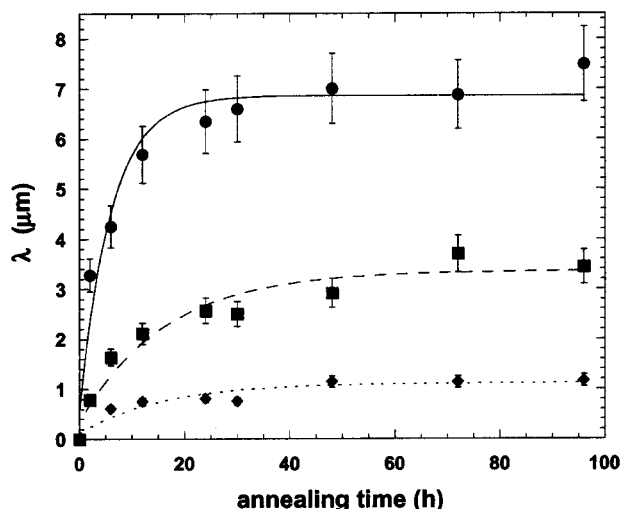


Figure 10. Plot of the average feature size, λ , versus annealing time, t , for the 26k (●, solid line), 51k (■, dashed line), and 104k (◆, dotted line) M samples showing how the pattern size becomes nearly stationary for long annealing times. The sample was annealed at 170 °C. The lines serve as guides for the eye, and error bars correspond to the standard uncertainty.

for all M values and times used. A similar cessation of growth of block copolymer surface features has been previously reported²⁶ where the size of holes and islands remained almost invariant for about 2 decades in annealing time. This cessation of growth of the surface pattern or “pinning” is indicative of viscoelastic restoring force in the block copolymers, and this will be explored further subsequently. A future article will further explore the kinetics of pattern evolution including the temperature dependence of the “pinned” value of λ and the characteristic time τ governing the approach to this steady state.⁴⁴

Another means of characterizing the effect of M on the surface-pattern morphology is by examining the roughness of the surface. The line profiles given in Figure 9 demonstrate the effect of M on the roughness. For the 6-h annealed data, the

low M sample [Fig. 9(a)] has relatively sharp corners in the line scan, whereas the corners for the higher M samples [Figs. 9(b,c)] are more rounded. With further annealing (30 h), the 54k sample [Fig. 9(e)] becomes sharper whereas the 104k sample [Fig. 9(f)] retains the rounding of the features. To quantify this, the root-mean-square roughness, r , [defined as $r = \sqrt{(\sum Z_i^2/N)}$, where Z_i is the difference in height from the mean value for each pixel, and N is the number of pixels] was calculated. The r values calculated from samples annealed for 6, 30, and 96 h are given in Table III. By normalizing r by L_o , the relative roughness of the different M samples can be compared, and these values are also given in Table III ($r/L_o = 0.5$ corresponds to a bicontinuous step function profile with two heights, $h = 0$ and $h = L_o$). This ratio shows that the high M sample has a less rough surface and that the corners of the patterns are rounded relative to the lower M samples. Thus, increasing the molecular mass at this modest annealing time decreases r on the scale of L_o , again indicative of viscoelastic effects in the block copolymers. Previous measurements¹³ have shown that the roughness of high M films changes slowly in time; thus, studies at very long times may be needed to confirm these roughness effects.

To further investigate the dependence of the surface-pattern morphology on M , a plot of λ as a function of L_o for representative films annealed 6 and 30 h is represented in Figure 11. We note the large scale of the surface patterns ($\lambda = 0.5\text{--}8\ \mu\text{m}$) in comparison with L_o and even the entire film thickness h .⁴⁵ The λ versus M data are nearly linear in a log–log plot and yield the scaling relation $\lambda\ (\mu\text{m}) \propto L_o^{-2.5}$ for all annealing times.⁴⁶ Using relation previously discussed, $\lambda \propto M^{0.66}$, λ has been found to scale with M according to the relation $\lambda\ (\mu\text{m}) \propto M^{-1.65}$.⁴⁷ The hole and island patterns that form for $h \neq h_c$ also remain stable (or at least evolve very slowly), and the average

Table III. Measured RMS Roughness Values for the AFM Micrographs in Figure 9 (Errors Given Are the Standard Uncertainty)

M_n (kg/mol)	r (6 h) (nm)	r (30 h) (nm)	r (96 h) (nm)	r/L_o (6 h)	r/L_o (30 h)	r/L_o (96 h)
26k	8.3 ± 0.2	8.3 ± 0.2	8.3 ± 0.2	0.47 ± 0.03	0.47 ± 0.03	0.47 ± 0.03
51k	13.1 ± 0.2	14.1 ± 0.2	13.9 ± 0.2	0.44 ± 0.02	0.47 ± 0.02	0.46 ± 0.02
104k	11.3 ± 0.2	15.5 ± 0.2	14.2 ± 0.2	0.27 ± 0.02	0.37 ± 0.02	0.34 ± 0.02

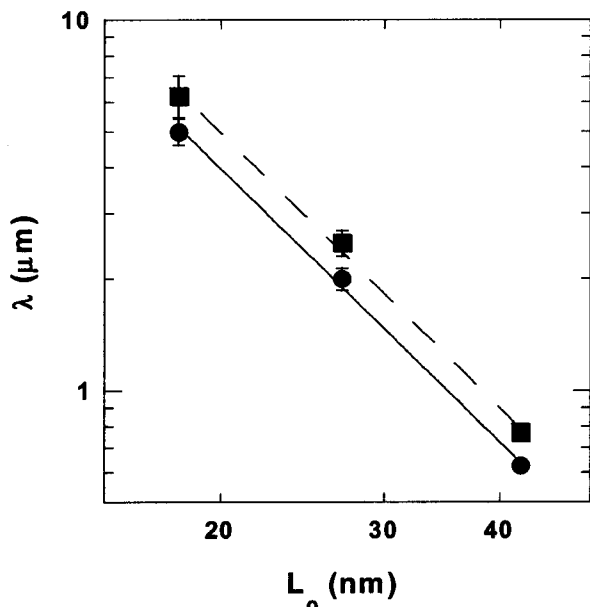


Figure 11. Size of labyrinthine pattern size, λ , versus bulk lamellar thickness, L_o , with standard uncertainties displayed. Data obtained for samples annealed for 6 h (●, solid line) and 30 h (■, dashed line) (Fig. 9) show a decrease in the lateral pattern size with M . Solid lines are power-law fits of the data yielding λ (μm) $\approx 7200L_o^{-2.5}$.

size of these morphological features likewise diminishes strongly with increasing M .

Utilizing this dependence of λ on M , we now return to the observation in Figure 8 that higher M films could sustain surface pattern formation with a higher ϵ . Specifically, the critical gradient, ϵ_c , where the width of the smooth region w_s becomes comparable to w_L , increases strongly with increasing M . This phenomenon is understandable given that the existence of a surface pattern requires that the difference $w_L - w_s$ must be larger than the minimal surface-pattern size. The sizes of the islands, holes, and spinodal patterns all have a comparable order of magnitude in our measurements (for fixed M) so that λ calculated previously can be approximately identified with this minimal pattern size. Thus ϵ_c can be expected to vary in some inverse relation to λ . Figure 12 shows a plot of ϵ_c versus λ , and the limited data suggest a nearly linear relation, $\epsilon_c \approx -470\lambda + 3600$ where the slope is notably negative.⁴⁶ Thus, the parameters λ and ϵ_c are indeed strongly correlated. Alternatively, a plot (not shown) of ϵ_c versus M indicates the approximate scaling $\epsilon_c \sim -aM^{-1.5} + 3500$, where a is a positive constant ($\approx 1.2 \times 10^{10}$). This relation suggests a tendency of ϵ_c to saturate at a constant value for high M .

DISCUSSION

The aforementioned observations raise questions about the nature of surface-pattern formation in block copolymer films that have not been previously addressed. At this point, we summarize our tentative views about the physical origin of the surface features observed in block copolymer thin films. These arguments provide a working model for understanding our data and guiding further measurements.

Brush Interpretation of Smooth Region

Previous studies⁴⁸ on the formation of polymer brush layers grafted in a poor solvent and dried in air have found a progression from island to labyrinthine to hole-surface patterns and finally smooth polymer films with an increase in the surface density, σ , of the grafted polymer chains. The *outer layer* of block copolymer films exposed to air can likewise be considered a brushlike layer with thickness, h_l , where the extended smooth regions about h_s of the block copolymer films correspond to h ranges where σ is relatively high. For films with $h < h_s$, σ should be smaller than that found in a “complete” lamella ($h = h_s$). Interchain interactions must be relatively weak in this regime, and the chain conformations within

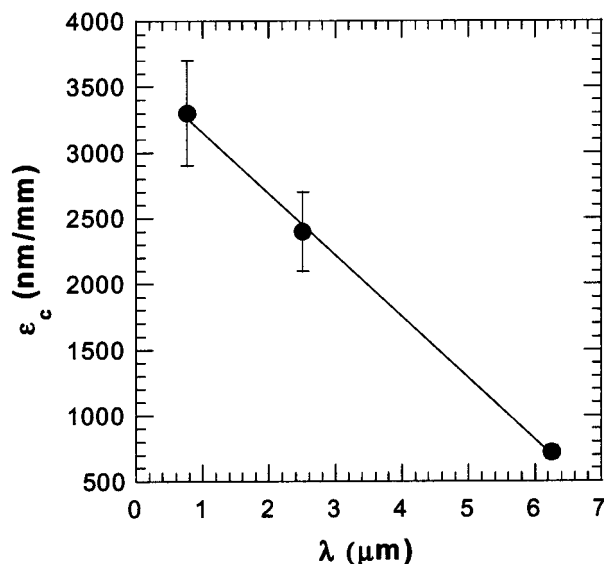


Figure 12. Plot of ϵ_c versus λ for the molecular mass polymers used here with the standard uncertainties given. The value of ϵ where the island and hole morphology disappear is linearly dependent on the average feature size of the spinodal pattern.

the “chain-deficient” block copolymer regime is expected to correspond to weak segregation scaling ($h_l \sim M^{1/2}$). In contrast, an increase of h above h_s should lead to an increase in σ and a further stretching of the outer chain layer into an extended “brushlike” form. We then expect the layer height of the outer block copolymer for $h > h_s$ to have a strong segregation scaling ($h_l \sim \alpha M^{0.66}$), but with a prefactor α different¹⁴ from the scaling relation for the bulk lamellar thickness $L_o \sim \alpha_e M^{0.66}$.

The stretching of the outer block copolymer layer between h_s and the swollen edge of the smooth band equals $(\alpha - \alpha_e)L_o$, and this stretching in comparison to the equilibrium layer thickness should be *constant* $(\alpha - \alpha_e)/\alpha_e$ in a fully developed scaling limit ($h_l \sim \alpha M^{0.66}$), where α is independent of M .⁴⁹ Previously, it was found that the height change relative to L_o measured from the center of the smooth region, $\delta h = (\Delta h/2)/L_o$, is nearly constant ($\delta h \approx 0.12$ – 0.14) in our measurements, in accord with these scaling arguments. The existence of chain stretching for $h_l > L_o$ is supported by previous results from Russell et al.²⁰ who directly observed significant swelling in the outer block copolymer layer based on a (single) neutron reflection measurement on a film of constant thickness where h exceeded h_s by 13% L_o . The stretching of the outer layer was also observed by de Jeu et al.⁵⁰ but on a smaller scale ($\approx 2\%$ L_o). The continuous change in the color of the smooth film region OM micrographs shown in Figure 6 provides evidence for a gradient in film thickness in these smooth film regions. This h gradient is attributed to a continuous transition from compressed to stretched chains within the outer block copolymer layer. We next focused on the topographic patterns observed for the remainder of the block copolymer thickness ranges.

Phase-Separation Model of Block Copolymer Surface-Pattern Formation

A number of researchers have suggested that the ordering of block copolymer films can be described by two-dimensional “phase separation”^{16,24,40–42} based on a phenomenological similarity of the surface-pattern growth in the block copolymer films to phase separation in fluid mixtures. In this model, the film height relative to a critical value defines an order parameter for the phase transition. The counterpart order parameter in fluid-phase separation is the composition relative to the critical composition.⁵¹ Although this picture

remains highly conjectural, it does have implications relevant to our measurements. This phase-separation model implies the formation of “spinodal decomposition” patterns for h near some critical height and formation of holes and islands structures for h greater or less than this critical height.⁴⁰ The block copolymer holes and islands correspond to droplet formation in off-critical fluid mixtures. This predicted behavior is remarkably consistent with our observations where h_c is identified with the critical height in the phase-transition model. In this type of picture, the observed deviation of h_c from $(m + 1)L_o$ for this copolymer seems to correspond to an asymmetric phase boundary (critical relative composition $\neq 0.5$). The phase-separation model of block copolymer pattern formation further suggests that the surface patterns in block copolymer films should morphologically resemble phase separation of “ultrathin” polymer blend films (where phase separation occurs quasi-two-dimensionally within the plane of the film). In studies of these blends, a progression from islands to spinodal to hole patterns with varying compositions is indeed observed,⁴⁸ and the morphology appears similar in form to the block copolymer surface patterns. We take this observation as encouraging evidence in qualitative support of the phase-separation model of surface-pattern formation in block copolymer films.

Surface Elasticity and Pattern Pinning

Our measurements on the block copolymer pattern formation have shown that the size of the patterns “pins” at long timescales (i.e., patterns stop growing). The effect has also been observed in phase-separating blend films,^{52,53} although the origin of the pinning may be quite different in these liquid-like systems. Surface elasticity has been suggested to play a large role in determining the scale and form of surface patterns in phase separating fluids when long-range interactions are present.^{54,55} In addition, this type of model (phase separation plus surface elasticity) has been invoked to rationalize pattern formation in the lipid bilayer films arising in cell membranes.^{54,55} The phase-separation model of block copolymer pattern formation discussed previously along with a generalization to account for film elasticity then has potential for guiding understanding of the observed M dependence of the spinodal pattern scale, λ .

To explore this interpretation of the surface-pattern formation, preliminary calculations of phase separation with surface elasticity were performed based on a Cahn–Hilliard model of phase separation and the Helfrich model of surface elasticity.⁵⁶ These calculations indicate that the presence of a finite-surface elastic constant, κ , can “pin” the scale of the phase separation over appreciable timescales. The surface elasticity of the film inhibits long wavelength phase separation much like the forming of the chemical junction in the block copolymer leading to an elastic restoring force acting against macroscopic phase separation. These calculations also indicate that if κ is not sufficiently large, the observed pinning is transient in nature, and growth will continue at long times. Because a similar “pinning” in the block copolymer surface patterns is observed, surface elasticity is then implicated as a potentially important parameter in the pattern formation of block copolymer films.

Inclusion of surface elasticity as a significant parameter in block copolymer pattern formation directly leads to specific expected behavior that can be studied. First, an increase in the surface elasticity is anticipated to decrease the surface roughness because of the larger energetic cost of chain displacements away from the average layer height. This is observed as rounding of the high M plateau features in Figure 9 and the decreasing value of r/L_o in Table III.⁵⁷ As the surface elasticity increases with increasing M , it is more difficult to form the sharp plateau boundaries because of the increased bending modulus. In addition, a larger bending modulus should result in a larger areal compressibility modulus, which in a simple mechanical model of a membrane is proportional to the bending modulus.^{58,59} This increased areal compressibility modulus leads us to expect that the formation of shallow surface patterns over large areas of the film surface requiring large-scale inplane displacements should likewise decrease with increasing surface elasticity. The increased elasticity acts as a restoring force to inhibit molecular migration over the length scales necessary to form large-scale patterns. This behavior is indeed observed in Figures 9, 10, and 11 for the block copolymer patterns. (Large-scale labyrinthine patterns are also observed in thin films of (neutral) gels exposed to a poor solvent, and the inplane size of the patterns decreases with increasing crosslink density similar to the outer block copolymer layer observed here.⁶⁰) To further understand the M dependence

of the block copolymer surface patterns, we next investigate the M dependence of κ and the dependence of the surface pattern scale λ on κ .

The surface rigidity, κ , of block copolymer layers has been theoretically predicted⁶¹ to increase strongly with M . We propose that the decrease in λ with an increase in M arises from the increasing energetic cost of the surface deformation as a result of the increasing elasticity that accompanies surface-pattern formation. Specifically, the preceding observations and discussions suggest an inverse relation between λ and κ , and we assume an inverse power relation, $\lambda \sim \kappa^{-\beta}$, where $0 < \beta < 1$. This relation is consistent with the observations that the patterns become large in low M films where the surface elasticity should be smaller. For strong segregation block copolymer layers⁶¹ and dense low molecular mass surfactant layers,⁶² κ is predicted to scale as $\kappa \sim M^{-3}$. By applying this relation to the current block copolymer study, the measurements of the previous section where $\lambda \sim M^{-1.65}$ yield the preliminary indication that β is near $\frac{1}{2}$, that is, $\beta \approx 0.55$.⁴⁷ Direct measurements of κ for the block copolymers used in the present work would be helpful in better establishing the relation between λ and κ , however.⁶² The increase of ε_c with increasing M in Figure 8 is also interpreted to arise from the increasing elasticity of the block copolymer layer with increasing M .⁵⁷ Films having a higher M are more elastic allowing for a more gradual bending of the free boundary on the scale of the surface pattern λ , which in turn allows the film to support larger h gradients.

The importance of surface elasticity in block copolymer pattern formation can be further demonstrated by additional observations. A change of the block copolymer monomer structure from the relatively rigid (PS-*b*-PMMA) to the more flexible PS-*b*-poly(*n*-butyl methacrylate) has been observed⁴² to give a large increase of the block copolymer pattern scale. These data are interpreted as an increase in pattern scale as a result of a reduced surface rigidity. Temperature measurements are also informative about the surface-pattern scale and origin. In a companion study,⁴⁴ a dramatic increase of the block copolymer pattern size is observed upon approaching the estimated film-ordering transition temperature. This observation is consistent with our hypothesis that surface elasticity (bending and compressional) controls pattern size because fluctuation effects near the ordering temperature should diminish κ and thus increase the size of the surface patterns.^{63,64}

Compositional fluctuations should also have the additional effect of slowing down the rate at which the surface patterns form near the surface-ordering transition (termed “phase-coherence transition” by Mansky et al.⁴²), and this effect has also been observed.^{63,64} These observations strongly suggest that surface elasticity and compositional fluctuations associated with the surface-ordering transition have a large influence on surface-pattern formation in thin block copolymer films. These effects should be investigated more thoroughly, both experimentally and theoretically.

Future Considerations

As a final point, recent work⁶⁵ on the modeling of pattern formation in block copolymer films predicts the formation of spiral patterns and other features not seen in our measurements. However, this modeling assumes the presence of strong hydrodynamic interactions in idealized two-dimensional block copolymer films. The importance of hydrodynamic interactions in ordered films with surface elasticity seems doubtful, but this model has potential interest in the *disordered regime* where the block copolymer film is more fluidlike in its viscoelastic properties. It would then be interesting to make films in the disordered regime to check if qualitatively different block copolymer patterns are then observed. In the disordered state, the surface viscosity^{66,67} should play a large role in the rate at which the surface patterns grow. Recent measurements,⁶⁸ of the surface viscosity, η_s , of homopolymer films indicate a scaling relation $\eta_s \sim M^{1.3}$, suggesting that there would be a strong reduction in the rate of growth of the patterns with increasing M . Block copolymer pattern formation in the disordered regime would be an interesting topic for a future investigation by combinatorial methods.

CONCLUSIONS

High-throughput methods are used to examine the properties of block copolymer thin films. Our method involves creating controlled, continuous gradients in film thickness using a specially designed automated flow coater and performing high-throughput characterization on these polymer films as a function of thickness, thickness gradient, and molecular weight. Automated analyses of the data generated by these libraries pro-

vides greatly enhanced experimental efficiency, providing samples with a large number of independent state points. The film gradient library information is validated through comparison to previous observations on surface-pattern formation in symmetric diblock copolymer films. This illustrative example shows the efficiency of the combinatorial method in exploring a complex physical phenomenon.

A single thickness gradient library reproduces the entire range of surface pattern formation, and new phenomena are identified in the process (formation of smooth films for extended thickness ranges and labyrinthine surface-pattern formation separating the familiar island and hole patterns). We attribute the thickness ranges where the film remains smooth to an increase of the surface chain density of the brushlike outer block copolymer layer with an increase in the film thickness. In this view, the smooth block copolymer films observed correspond to the last stage of brush formation where the brush layer is continuous, but increasingly filled as the film thickness increases. The scaling relation for the stretched chains in the overfilled layers ($h \geq h_s$) is believed to still obey the strong segregation scaling relation ($h_l \sim \alpha M^{2/3}$) but with an altered limiting prefactor α at the edge of the band where the maximum extension is presumed to occur. This argument indicates that the extent of layer stretching across a band should be a constant fraction of L_o , in accord with our measurements. Specifically, the height change across the smooth regions, normalized by L_o , was found to be nearly independent of molecular mass and the magnitude of the surface gradient (provided the gradient was small enough to geometrically accommodate surface patterns). Once the gradient slope became sufficiently large, these smooth regions increasingly dominated the morphology until above a critical slope a step-like morphology was adopted. This critical slope is found to vary linearly with pattern dimension.

The size and evolution of the block copolymer surface patterns at long times were also investigated. The average sizes of these patterns are found to become nearly stationary at long annealing times with the larger M samples have a significantly smaller size. The average size of the spinodal block copolymer pattern was found to scale as $\lambda \sim L_o^{-2.5}$ (or equivalently $\lambda \sim M^{-1.65}$). This effect is attributed to a strong increase in the surface elasticity of the outer block copolymer layer with M and the increased energetic cost of

large-scale surface deformation accompanying surface pattern formation. These observations provide a confirmation of the value of combinatorial methodology to rapidly explore complex phenomena dependent on many relevant variables, validating the technique against previous measurements and showing the power of the methodology to identify new and important phenomena even in mature fields of polymer science.

The authors thank Dr. M. VanLandingham for use of and assistance with the AFM. The authors also acknowledge the helpful discussions with Drs. P. Green and I. Szleifer about block copolymer film morphology and surface elasticity, respectively.

APPENDIX: INTERPRETATION OF CRITICAL LAYER THICKNESS, H_C

The formation of island, hole, and complex cluster patterns is a ubiquitous phenomenon in the formation of self-assembled monolayers,^{69–71} the growth of grafted polymer layers,⁴⁸ and the surface structure of growing or melting crystals.⁷² Although the growth of the outer block copolymer layer is phenomenologically similar to the formation of physisorbed grafted polymer layers, we can also draw an analogy to the growth of crystals where hole and island features form near the crystal surface even near equilibrium and where the interaction between the ordered layers within the crystal and the crystal surface is important.⁷² We may consider ordered block copolymer films as varieties of smectic phases similar to those observed in liquid crystals. The viewpoint of surface-pattern formations as a variety of “surface roughening” in block copolymer crystals has some interesting implications. The equilibrium features of the surface-pattern formation should be very dependent on T , and we can expect the surface-pattern properties to be described by a phase transition in some cases.⁷² The type of surface-phase transition (second or infinite order) or even whether a thermodynamic phase transition exists at all depends on the energetic asymmetry of forming island and hole structures in the outer crystal layer.⁷² The nature of the order–disorder surface “roughening transition” is somewhat specific to the molecular structure of the crystallizing species.

As previously mentioned, the observed deviation of h_c from $(m + 1)L_o$ for this copolymer seems to correspond to an asymmetric phase

boundary (critical relative composition $\neq 0.5$). This asymmetry arises from a breaking of the exchange symmetry between the fluid particles in fluid mixtures and the breaking of the “particle hole” symmetry in the spin model of crystal roughening.⁷² In the case of crystals, the symmetry breaking is associated with an energetic inequivalence between the formation of island and hole-surface patterns having the same shape and size.⁷² As previously mentioned, this symmetry breaking has important ramifications for the nature of the surface-roughening transition. An energetic asymmetry between the formation of islands and holes has been predicted to act like an applied field. Thus, the surface-roughening transition near the ordering transition becomes “rounded” (no phase transition exits), leading to a tendency of the crystal surface to gradually change from smooth to rough over a large temperature range.⁷²

REFERENCES AND NOTES

1. Terret, N. K. *Combinatorial Chemistry*; Oxford University Press: Oxford, England, 1998.
2. Czarnik, A. W.; Dewitt, S. H. *A Practical Guide to Combinatorial Chemistry*; American Chemical Society: Washington, DC, 1997.
3. Borman, S. *Chem Eng News* 1999, 77, 33.
4. Gordon, E. M.; Kerwin, J. F. *Combinatorial Chemistry and Molecular Diversity in Drug Discovery*; Wiley: New York, 1998.
5. Jandeleit, B.; Schaefer, D. J.; Powers, T. S.; Turner, H. W.; Weinberg, W. H. *Angew Chem Int Ed Engl* 1999, 38, 2494.
6. Drolet, F.; Fredrickson, G. H. *Phys Rev Lett* 1999, 83, 4317.
7. Meredith, J. C.; Smith, A. P.; Karim, A.; Amis, E. J. *Macromolecules* 2000, 33, 9747.
8. Meredith, J. C.; Karim, A.; Amis, E. J. *Macromolecules* 2000, 33, 5760.
9. Smith, A. P.; Meredith, J. C.; Douglas, J. F.; Amis, E. J.; Karim, A. *Phys Rev Lett* 2001, 87.
10. Hasegawa, H.; Hashimoto, T. *Macromolecules* 1985, 8, 589.
11. Henkee, C. S.; Thomas, E. L.; Fetters, L. J. *J Mater Sci* 1988, 23, 1685.
12. Green, P. F.; Christensen, T. M.; Russell, T. P.; Jerome, R. *Macromolecules* 1989, 22, 2189.
13. Russell, T. P.; Coulon, G.; Deline, V. R.; Miller, D. C. *Macromolecules* 1989, 22, 4600.
14. Anastasiadis, S. H.; Russell, T. P.; Satija, S. K.; Majkrzak, C. F. *J Chem Phys* 1990, 92, 5677.
15. Ausserre, D.; Chatenay, D.; Coulon, G.; Collin, B. *J Phys (Paris)* 1990, 51, 2571.

16. Coulon, G.; Ausserre, D.; Russell, T. P. *J Phys (Paris)* 1990, 51, 777.
17. Coulon, G.; Collin, B.; Ausserre, D.; Chatenay, D.; Russell, T. P. *J Phys (Paris)* 1990, 51, 2801.
18. Green, P. F.; Christensen, T. M.; Russell, T. P.; Jerome, R. *J Chem Phys* 1990, 92, 1478.
19. Green, P. F.; Christensen, T. M.; Russell, T. P. *Macromolecules* 1991, 24, 252.
20. Russell, T. P.; Menelle, A.; Anastasiadis, S. H.; Satija, S. K.; Majkrzak, C. F. *Macromolecules* 1991, 24, 6263.
21. Collin, B.; Chatenay, D.; Coulon, G.; Ausserre, D.; Gallot, Y. *Macromolecules* 1992, 25, 1621.
22. Menelle, A.; Russell, T. P.; Anastasiadis, S. H.; Satija, S. K.; Majkrzak, C. F. *Phys Rev Lett* 1992, 68, 67.
23. Russell, T. P.; Menelle, A.; Anastasiadis, S. H.; Satija, S. K.; Majkrzak, C. F. *Makromol Chem Macromol Symp* 1992, 62, 157.
24. Bassereau, P.; Brodbreck, D.; Russell, T. P.; Brown, H. R.; Shull, K. R. *Phys Rev Lett* 1993, 71, 1716.
25. Cai, Z.; Huang, K.; Montano, P. A.; Russell, T. P.; Bai, J. M.; Zajac, G. W. *J Chem Phys* 1993, 93, 2376.
26. Coulon, G.; Collin, B.; Chatenay, D.; Gallot, Y. *J Phys II (Paris)* 1993, 3, 697.
27. Coulon, G.; Daillant, J.; Collin, B.; Benattar, J. J.; Gallot, Y. *Macromolecules* 1993, 26, 1582.
28. Mayes, A. M.; Russell, T. P.; Bassereau, P.; Baker, S. M.; Smith, G. S. *Macromolecules* 1994, 27, 749.
29. Grim, P. C. M.; Nyrkova, I. A.; Semenov, A. N.; ten Brinke, G.; Hadziioannou, G. *Macromolecules* 1995, 28, 7501.
30. Mansky, P.; Russell, T. P.; Hawker, C. J.; Pitsikalis, M.; Mays, J. *Macromolecules* 1997, 30, 6810.
31. Mansky, P.; Russell, T. P.; Hawker, C. J.; Mays, J.; Cook, D. C.; Satija, S. K. *Phys Rev Lett* 1997, 49, 237.
32. Heier, J.; Sivaniah, E.; Kramer, E. J. *Macromolecules* 1999, 32, 9007.
33. Heier, J.; Genzer, J.; Kramer, E. J.; Bates, F. S.; Walheim, S.; Krausch, G. *J Chem Phys* 1999, 111, 11101.
34. Certain equipment and instruments or materials are identified in this article to adequately specify the experimental details. Such identification does not imply recommendation by the National Institute of Standards and Technology, nor does it imply the materials are necessarily the best available for the purpose.
35. Kern, W. *Handbook of Semiconductor Wafer Cleaning Technology*; Noyes Data: Park Ridge, NJ, 1993.
36. Fluid transport will cause the thickness gradient to equilibrate and form a uniform film. The timescale and lengthscale over which gradient library measurements are valid are limited by the rate of transport. In most cases, high M polymers are utilized that have relatively low diffusivity and high viscosity in their fluid state. Block copolymer materials have a gel-like viscoelasticity in the ordered regime. Thus, the diffusive and convective flow length and timescales for the relaxation of the film h gradient are often orders of magnitude lower than those of the measurements, allowing properties to be studied near equilibrium for the annealing times used. As a check for flow-induced leveling, four thickness gradient libraries of low molecular mass PS were examined before and after annealing.⁷ The difference in the thickness gradient measured before and after annealing was equal within standard uncertainty. Similar stability of the block copolymer gradients utilized here is expected.
37. According to ISO 31-8, the term "molecular weight" has been replaced by "relative molecular mass," M_r . The conventional notation, rather than the ISO notation, has been used for this publication.
38. Utracki, L. A. *Polymer Alloys and Blends*; Hanser: Munich, 1990; pp 45–52.
39. Xie, R.; Karim, A.; Douglas, J. F.; Han, C. C.; Weiss, R. *Phys Rev Lett* 1998, 81, 1251. In the modeling of dewetting as a spinodal decomposition process, the height of the film is an order of parameter-like variable. See: Vrig, A. *Discuss Faraday Soc* 1996, 42, 23.
40. Joly, S.; Raquois, A.; Paris, F.; Hamdoun, B.; Avray, L.; Ausserre, D.; Gallot, Y. *Phys Rev Lett* 1996, 77, 4394. The critical height defining the height-order parameter in this model is defined as $h_s = (m + \frac{1}{2})L_o$ rather than h_c . The existence of spinodal patterns was not inferred by these researchers, but these structures seem to be implicit in the type of model they propose.
41. Vignaud, G.; Gibaud, A.; Grubel, G.; Joly, S.; Ausserre, D.; Legrand, J. F.; Gallot, Y. *Phys Status Solidi B* 1998, 248, 250.
42. Mansky, P.; Tsui, O. K. C.; Russell, T. P.; Gallot, Y. *Macromolecules* 1999, 32, 4832.
43. Ohta, T.; Kawasaki, K. *Macromolecules* 1986, 19, 2621.
44. Smith, A. P.; Douglas, J. F.; Amis, E. J.; Karim, A. in preparation 2001.
45. Similar large-scale labyrinthine surface patterns have been observed in liquid-crystal thin films, and we suggest these may have a similar origin to the block copolymer patterns observed here. See: (a) Vandenbrouck, F.; Valignat, M. P.; Cazabat, A. M. *Phys Rev Lett* 1999, 82, 2693; (b) Herminghaus, S.; Jacobs, K.; Mecke, K.; Bischof, J.; Fery, A.; Ibn-Elhaj, M.; Schlagowski, S. *Science* 1998, 282, 916.
46. As a result of the limited data available, it is difficult to quantify the uncertainty.
47. A direct plot of λ versus M based on the limited number of M values yields $\lambda \sim M^{-1.5}$ correspond-

- ing to $\beta = 0.5$. The discrepancy reflects the uncertainty in our data.
48. Karim, A.; Tsukruk, V. V.; Douglas, J. F.; Satija, S. K.; Fetters, L. J.; Reneker, D. H.; Foster, M. D. *J Phys II (Paris)* 1995, 5, 1441. The hole patterns found beyond the labyrinthine pattern regime are not shown in this article.
 49. Adamuti-Trache, M.; McMullen, W. E.; Douglas, J. F. *J Chem Phys* 1996, 105, 4798.
 50. de Jeu, W. H.; Lambooy, P.; Vaknin, D. *Macromolecules* 1993, 26, 4973.
 51. Glotzer, S. C. *Annual Reviews of Computational Physics* 1995, 2, 1. See numerous references cited in this work.
 52. Sung, L.; Karim, A.; Douglas, J. F.; Han, C. C. *Phys Rev Lett* 1996, 76, 4368.
 53. Ermi, B. D.; Karim, A.; Douglas, J. F. *J Polym Sci B: Polym Phys* 1998, 36, 191.
 54. Leibler, S.; Andelman, D. *J Phys (Paris)* 1987, 48, 2013.
 55. Seul, M.; Andelman, D. *Science* 1995, 267, 476.
 56. Jiang, Y.; Lookman, T.; Sayers, A. B.; Douglas, J. F. in preparation. The Cahn–Hilliard model of phase separation in combination with the Helfrich model of the surface elasticity shows that the scale of the film phase separation pattern “pins” at long times because of surface elasticity. See also: (a) Jaing, Y.; Lookman, T.; Saxena, A. *Phys Rev E: Stat Phys Plasmas Fluids Relat Interdiscip Top* 2000, 61, R57; (b) Seul, M.; Andelman, D. *Science* 1995, 267, 476. There are also interesting simulations of elastic effects in alloy-phase separation (Onuki, A.; Nishimori, H. *Physical Review B Condensed Matter and Materials Physics* 1991, 43, 13649) that show that elasticity can modify the coarsening dynamics from the conventional one-third scaling of “ordinary” phase separation. Smaller apparent exponents are reported in this work.
 57. The decreased roughness of the high M films is influenced by kinetic effects that seem to evolve over long timescales.
 58. Evans, E.; Rawicz, W. *Phys Rev Lett* 1990, 64, 2094.
 59. Discher, B. M.; Won, Y. Y.; Ege, D. S.; Lee, J. C. M.; Bates, F. S.; Discher, D. E.; Hammer, D. A. *Science* 1999, 284, 1143. These researchers recently reported the first measurements of the bending and compressional moduli of block copolymer films of polymersome vesicles.
 60. Horkay, F. National Institute of Health, Bethesda, MD. Personal communication (2001).
 61. Wang, Z. G.; Safran, S. A. *J Chem Phys* 1991, 94, 679.
 62. Wurger, A. *Phys Rev Lett* 2000, 85, 337.
 63. Helfrich, W. *J Phys France* 1985, 46, 1263.
 64. Peliti, L.; Leibler, S. *Phys Rev Lett* 1985, 54, 1690.
 65. Shiwa, Y. *Phys Rev E: Stat Phys Plasmas Fluids Relat Interdiscip Top* 2000, 61, 2924.
 66. Wasan, D. T.; Gupta, L.; Vora, M. K. *AIChE J* 1971, 17, 1287.
 67. Wasan, D. T.; McNamara, J. J.; Shah, S. M.; Sampath, K. J. *J Rheol* 1979, 23, 181.
 68. Sato, N.; Ito, S.; Yamamoto, M. *Macromolecules* 1998, 31, 2673.
 69. Doudevski, I.; Schwartz, D. K. *Physical Review B Condensed Matter and Materials Physics* 1999, 60, 14.
 70. Woodward, J. T.; Doudevski, I.; Sikes, H. D.; Schwartz, D. K. *J Phys Chem B* 1997, 101, 7535.
 71. Roder, H.; Hahn, E.; Brune, H.; Bucher, J.; Kern, K. *Nature* 1993, 366, 141.
 72. Rys, F. S. *Phys Rev Lett* 1986, 56, 624.